Transport in Porous Media **20:** 197–221, 1995.

Modeling of Colloid and Colloid-Facilitated Contaminant Transport in a Two-Dimensional Fracture with Spatially Variable Aperture

ASSEM ABDEL-SALAM and CONSTANTINOS V. CHRYSIKOPOULOS*
Department of Civil and Environmental Engineering, University of California, Irvine, CA 92717, U.S.A.

(Received: 16 February, 1994; in final form: 3 March, 1995)

Abstract. Mathematical models are developed for two-dimensional transient transport of colloids, and cotransport of contaminant/colloids in a fracture-rock matrix system with spatially variable fracture aperture. The aperture in the fracture plane is considered as a lognormally distributed random variable with spatial fluctuations described by an exponential autocovariance function. Colloids are envisioned to irreversibly deposit onto fracture surfaces without penetrating the rock matrix; whereas, the contaminant is assumed to decay, sorb onto fracture surfaces and onto colloidal particles, as well as to diffuse into the rock matrix. The governing stochastic transport equations are solved numerically for each realization of the aperture fluctuations by a fully implicit finite difference scheme. Emphasis is given on the effects of variable aperture on colloid and colloid-facilitated contaminant transport. Simulated breakthrough curves of ensemble averages of several realizations show enhanced colloid transport and more pronounced fingering when colloids are subject to size exclusion from regions of small aperture size. Moreover, it is shown that an increase in the fracture aperture fluctuations leads to faster transport and increases dispersion. For the case of contaminant/colloids cotransport it is shown, for the conditions considered in this work, that colloids enhance contaminant mobility and increase contaminant dispersion.

Key words: Colloid transport, contaminant transport, single fracture, variable aperture, size exclusion, stochastic modeling.

Nomenclature

b	fracture aperture, L
c	contaminant concentration in the fracture, M/L^3
c_m	contaminant concentration in the rock matrix, M/L^3
c_o	source contaminant concentration, M/L^3
c^*	contaminant concentration adsorbed onto fracture surfaces, M/L^2
c_m^*	contaminant concentration adsorbed inside the rock matrix, M/M
d_p	colloidal particle diameter, L
$\mathbf{D}$	hydrodynamic dispersion coefficient dyadic, L^2/t
$\mathcal{D}$	Brownian diffusion coefficient for colloids and molecular diffusion coefficient for contaminants, L^2/t
$\mathcal{D}_m$	effective diffusion coefficient in the rock matrix, L^2/t

* Author to whom correspondence should be addressed

h total head potential in the fracture, L
K_f partition coefficient for contaminant sorption onto fracture surfaces, L
K_m contaminant partition coefficient in the rock matrix, L^3/M
K_n partition coefficient for contaminant sorption onto suspended colloids, L
K_{n^*} partition coefficient for contaminant sorption onto deposited colloids, L^3/M
ℓ_x fracture length in the x-direction, L
ℓ_y fracture length in the y-direction, L
n colloid concentration in the liquid phase, M/L^3
n_o source colloid concentration, M/L^3
n^* colloid concentration adsorbed onto fracture surfaces, M/L^2
$n^*_{\max}$ maximum deposited colloid concentration on fracture surfaces, M/L^2
N^* number of deposited colloidal particles per unit surface area of the fracture, $1/L^2$
$N^*_{\max}$ maximum number of deposited colloidal particles per unit surface area of the fracture, $1/L^2$
q^* diffusive mass flux into the rock matrix, M/L^2t
R retardation factor in the fracture
R_m retardation factor in the rock matrix
s contaminant concentration adsorbed on colloids in the liquid phase, M/M
s_o source solid-phase contaminant concentration onto suspended colloids, M/M
s^* contaminant concentration adsorbed on deposited colloids, M/M
t time, t
$\mathbf{U}$ interstitial velocity vector, L/t
x coordinate along the fracture length, L
y coordinate along the fracture width, L
z coordinate perpendicular to the fracture plane, L
α area blocked by a deposited colloidal particle, L^2
α_L longitudinal dispersivity, L
α_T transversal dispersivity, L
γ fluid specific weight, M/L^2t^2
ϵ fraction of the fracture surface physically covered by colloids
ζ dummy integration variable
θ porosity of the rock matrix
κ colloid deposition coefficient, L
λ first-order decay coefficient, 1/t
μ fluid dynamic viscosity, M/Lt
ξ defined in (18)
ρ_b bulk density of the rock matrix, M/L^3
ρ_p colloidal particle density, M/L^3
σ standard deviation of the lognormally distributed fluctuations of the fracture aperture

1. Introduction

The disposal of hazardous wastes, particularly those related to radioactive underground repositories in deep, fractured low permeability rocks (e.g., granites, slates, and gneisses) has stimulated the interest of many researchers to study contaminant migration in such types of rocks (e.g., Neretnieks *et al.*, 1982; Abelin, 1986; Raven *et al.*, 1988; Haldeman *et al.*, 1991; Johns and Roberts, 1991; Krishnamoorthy, *et al.*

1992). In these studies, contaminant transport is modeled assuming that dissolved species may sorb onto the immobile solid phase associated with fracture surfaces, and may diffuse into rock matrix micro-fissures. However, several experimental and field studies in fractured and porous media indicate that contaminants can also migrate adsorbed on the surface of colloid particles (e.g., Buddemeier and Hunt, 1988; Champ and Schroeter, 1988; Toran and Palumbo, 1992; Moulin and Ouzounian, 1992). For instance, plutonium and americium at two different sites at Los Alamos, New Mexico were detected at distances much farther than what predicted, and it was verified that these metals were carried by colloid particles (McCarthy and Zachara, 1989). At the Nevada test site, radionuclides were found to move outside a nuclear detonation cavity by transport on colloidal particles (Buddemeier and Hunt, 1988).

In modeling flow and contaminant transport in fractured rocks, the most common conceptual model employed by several researchers is a single fracture separated by a constant aperture, which is known as the parallel plate model (e.g., Grisak and Pickens, 1981; Neuzil and Tracy, 1981; Neretnieks, 1983; Novakowski *et al.*, 1985; Raven *et al.*, 1988; Shapiro and Nicholas, 1989, to mention a few representative studies). The shape of a fracture is primarily influenced by the mechanical properties of the rock, the geometric characteristics of the fracture surfaces, the relative displacement of the two surfaces, and the stress to which the rock is subjected to (Abelin, 1986). One of the problems associated with the parallel plate model is that it ignores the roughness, waviness, and tortuosity of the fracture surfaces (Schrauf and Evans, 1986). Moreover, at high normal stresses caused by the overburden pressure, fracture surfaces tend to close, the contact area between these surfaces increases and consequently the fracture aperture takes on a range of values rather than one single value (Moreno *et al.*, 1988).

Because the simplifying assumptions associated with the parallel plate model do not represent real rock fractures, several modifications have been proposed. A correction term is often included in the equation describing the flow in a fracture to account for surface roughness, absolute height of asperities (roughness perturbations in the fracture surface), and/or tortuosity of the flow (e.g., Witherspoon *et al.*, 1980; Neuzil and Tracy, 1981). Gale *et al.* (1985) indicated that a correction for roughness alone is not adequate for fractures with surfaces highly in contact, in which case preferential flow paths may occur. Preferential flow has been observed in several field and laboratory experiments (Neretnieks, 1985; Pyrak *et al.*, 1985; Abelin, 1986; Bourke, 1987; Haldeman *et al.*, 1991). Various conceptual models have been proposed in the literature for simulation of preferential flow in one- and two-dimensional variable aperture fractures (Tsang and Tsang, 1987; Moreno *et al.*, 1988).

Colloids are very fine particles that range in size between 10^{-3} and 1 μm (Buddemeier and Hunt, 1988). A wide variety of micro-organisms, organic, and inorganic colloidal material have been found in groundwaters. These may include clay minerals, metal oxides, viruses, bacteria, and organic macromolecules (e.g.,

humic substances) (Higgo *et al.*, 1993). Formation of mobile colloidal suspensions in subsurface formations can be attributed to a number of mechanisms: (1) matrix dissolution due to changes in pH or redox conditions; (2) supersaturation with respect to inorganic species; (3) disruption of the mineral matrix by large alterations in flow conditions due to injection, pumping or large rainfall infiltrations; (4) release and movement of viruses and bacteria; and (5) formation of micelles from the agglomeration of humic acids (Puls *et al.*, 1993). Colloids, both in the liquid-phase and fixed onto solid surfaces, have high specific surface area per unit mass; thus, they possess a high sorptive capacity for contaminants (e.g., Sposito, 1984; Enfield and Bengtsson, 1988; McCarthy and Zachara, 1989).

In order for colloids to considerably affect the transport of contaminants in the subsurface, the suspended colloidal concentration must be sufficiently high and stable (i.e., remain in suspension). Concentrations as high as 63 mg/l have been observed in some subsurface systems (Buddemeier and Hunt, 1988). The existence and persistence of stable colloidal suspensions depends on a combination of van der Waals attractive forces that promote aggregation, electrostatic repulsive forces that keep particles apart, and fluid chemistry. When electrostatic repulsions are dominant, especially at low ionic strengths, the particles are electrostatically stabilized and remain in a dispersed state (McCarthy and Zachara, 1989).

The presence of mobile colloidal suspensions can enhance the transport of contaminants, which might otherwise be retarded through conventional mechanisms. In addition to enhancing contaminant transport, certain types of colloids are also hazardous to human health (e.g., supersaturated nuclear species, microorganisms). Consequently, the first part of the paper is devoted solely to colloid transport in fractures. Moreover, the effect of colloid exclusion from areas of small aperture size on colloid transport and ultimately on contaminant transport is examined. This study of colloid exclusion was motivated by experimental observations of retardation factors with values < 1 (e.g., Champ and Schroeter, 1988; Enfield *et al.*, 1989; Harvey *et al.*, 1989; Toran and Palumbo, 1992). Finally, the impact of the presence of colloids on contaminant transport is investigated. The stochastic models derived in this paper describe colloid and contaminant transport in the presence of colloids within a two-dimensional fracture with spatially variable aperture. Colloid deposition onto fracture surfaces and contaminant diffusion into the rock matrix are incorporated into the transport models as first order processes. Contaminant sorption onto fracture surfaces, suspended and deposited colloids, and onto rock matrix solid surfaces is described by linear equilibrium isotherms. The reduction in contaminant matrix diffusion and fracture sorption, due to fracture surface area shrinkage caused by deposited colloids, is also accounted for.

2. Development of Models

2.1. FLOW MODEL

Realizations of the variable aperture field in the fracture plane are generated by the geostatistical code COVAR (Williams and El-Kadi, 1986), assuming that the fracture aperture is a stationary stochastic variable with a known probability density function and spatial correlation length. COVAR generates a covariance matrix, based on a preselected autocovariance function. The fracture plane is superimposed by a rectangular mesh of regular size, where each unit element enclosed by grid lines is assigned a different aperture. Flow in the rock matrix is neglected, because the saturated hydraulic conductivity in the rock matrix is several orders of magnitude smaller than the saturated hydraulic conductivity in the fracture (Streltsova, 1988).

The two-dimensional steady-state partial differential equation (pde) for flow in a spatially variable aperture fracture is derived from mass balance considerations over a fixed control fracture volume, and is given as

$$\frac{\partial}{\partial x}\left[b^3(x,y)\frac{\partial h(x,y)}{\partial x}\right] + \frac{\partial}{\partial y}\left[b^3(x,y)\frac{\partial h(x,y)}{\partial y}\right] = 0, \tag{1}$$

where b is the fracture aperture at a location (x, y); and h is the total head potential. For the derivation of the above equation it was assumed that the cubic law for incompressible laminar flow between two parallel plates (Schrauf and Evans, 1986) can simulate efficiently the flow through each unit element of the fracture. The preceding equation is a stochastic pde, because one of its parameters, namely b, is a stochastic variable. For each realization of the aperture field, a five-point central finite difference numerical approximation is employed for the solution of the governing flow equation (Lapidus and Pinder, 1982). The aperture at the interface of two adjacent elements in the x- and y-directions are obtained by employing the harmonic mean (Huyakorn and Pinder, 1983). The boundary conditions imposed on the flow model are: a constant head gradient with flow towards the right boundary, and impervious upper and lower boundaries. The resulting set of linear equations, with as many unknowns as the number of unit elements in the fracture, is solved using a banded LU decomposition matrix solver algorithm (Press *et al.*, 1992) to obtain the total head potential in every unit element. Velocity components in the x- and y-directions are then calculated for every unit element from the steady-state volumetric fluxes by the following expressions:

$$U_x = -\frac{b^2(x,y)\gamma}{12\mu}\frac{\partial h(x,y)}{\partial x}, \quad U_y = -\frac{b^2(x,y)\gamma}{12\mu}\frac{\partial h(x,y)}{\partial y}, \tag{2a, b}$$

where γ is the fluid specific weight; and μ is the fluid dynamic viscosity.

2.2. COLLOID TRANSPORT MODEL

The governing partial differential equation for colloid transport in a two-dimensional fracture with spatially variable aperture, assuming that colloids are stable and of equal size, is derived from mass balance considerations, and is given by

$$b(x,y)\frac{\partial n(t,x,y)}{\partial t}$$

$$= \nabla \cdot \left[b(x,y)\mathbf{D} \cdot \nabla n(t,x,y) - b(x,y)\mathbf{U}n(t,x,y)\right] - 2\frac{\partial n^*(t,x,y)}{\partial t}, \quad (3)$$

where n is the concentration of colloids suspended in the liquid phase; n^* is the concentration of colloids deposited on the fracture surfaces, expressed as mass of colloids per unit area of the fracture surface; t is time; ∇ is the two-dimensional vector gradient operator (del); $\nabla\cdot$ denotes divergence ($\nabla \cdot \mathbf{F} = \partial F_x/\partial x + \partial F_y/\partial y$, where $\mathbf{F}$ is an arbitrary two-dimensional vector); $\mathbf{U}$ is the interstitial flow velocity vector defined as

$$\mathbf{U} = \begin{pmatrix} U_x(x,y) \\ U_y(x,y) \end{pmatrix}, \quad (4)$$

where U_x and U_y are the velocity components in the x- and y-directions, respectively; and $\mathbf{D}$ is a 2×2 matrix of hydrodynamic dispersion coefficients

$$\mathbf{D} = \begin{pmatrix} D_{xx}(x,y) & D_{xy}(x,y) \\ D_{yx}(x,y) & D_{yy}(x,y) \end{pmatrix}, \quad (5a)$$

where each coefficient is defined by (Bear and Verruijt, 1987)

$$D_{pq} = \alpha_T \delta_{pq}(U_x^2 + U_y^2)^{1/2} + (\alpha_L - \alpha_T)\frac{U_p U_q}{(U_x^2 + U_y^2)^{1/2}} + \mathcal{D}, \quad (5b)$$

where α_L and α_T are the longitudinal and transversal dispersivities in the x- and y-directions, respectively; δ_{pq} is the Kronecker delta; and $\mathcal{D}$ is the Brownian diffusion coefficient for colloids; and the subscript $pq = xx$, xy, yx, or yy. It should be noted that for the derivation of (3) it is assumed that colloids do not penetrate into the rock matrix. This assumption is based on the work by Bowen and Epstein (1979) and Bradbury and Green (1986) who investigated the colloidal particle accessibility to several types of rock matrix pores and reported no colloidal penetration. In addition, it is assumed that no colloid mass is lost through particle straining (entrapment between the fracture surfaces).

Although microscopically the deposition of colloids is affected by many physicochemical processes, in order to model macroscopic colloid transport the following

phenomenological equation describing the mass flux of colloids onto the fracture surfaces is used

$$\frac{\partial n^*(t,x,y)}{\partial t} = \begin{cases} \kappa[U_x^2(x,y) + U_y^2(x,y)]^{1/2} \dfrac{n(t,x,y)}{b(x,y)}, & n^* < n^*_{\max} \\ 0, & n^* \geq n^*_{\max} \end{cases}, \quad (6)$$

where κ is the colloid deposition coefficient, which is a lumped parameter accounting for several colloid deposition mechanisms (i.e., Brownian diffusion, van der Waals forces, electric double layer forces); and $n^*_{\max}$ is the maximum deposited colloid concentration, which is a function of colloidal size and the number of available sites for colloid deposition. The above equation is based on the deep-bed filtration theory (Herzig *et al.*, 1970). Similar relationships have been used for colloid transport in porous media (e.g., Harvey and Garbedian, 1991). Champ and Schroeter (1988) indicated that the filtration process in fractured systems is similar to that found in a gravel aquifer. Bowen and Epstein (1979) provided a similar relationship to (6) for the deposition of colloids in fractured media. One of the limitations of (6) is that it does not account for the reduction in fracture permeability as a result of colloid deposition onto fracture surfaces.

The maximum deposited colloid concentration $n^*_{\max}$ is determined assuming that every deposited particle effectively blocks a certain area α of the fracture surface from further colloid deposition. This assumption has also been employed by Song and Elimelech (1993) for colloid transport in porous media. The area blocked by a colloid particle is a function of colloid diameter and the number of adsorption sites on the fracture surface. Knowing the area blocked by each deposited particle, the maximum number of colloids that can cover uniformly (i.e., square packing) every unit element in the fracture surface is determined. The deposited colloid concentration in the fracture domain is then calculated every time step and deposition is cut off from elements in the fracture where $n^* \geq n^*_{\max}$.

The necessary initial and boundary conditions for the physical system considered in this study are:

$$n(0,x,y) = 0, \quad (7a)$$

$$n(t,0,y) = n_o, \quad (7b)$$

$$\frac{\partial n(t,\ell_x,y)}{\partial x} = 0, \quad (7c)$$

$$-D_{yy}(x,0)\frac{\partial n(t,x,0)}{\partial y} + U_y(x,0)\, n(t,x,0) = 0, \quad (7d)$$

$$-D_{yy}(x,\ell_y)\frac{\partial n(t,x,\ell_y)}{\partial y} + U_y(x,\ell_y)\, n(t,x,\ell_y) = 0, \quad (7e)$$

where n_o is the constant colloid concentration at the source; and ℓ_x and ℓ_y are the dimensions of the fracture in the x- and y-directions, respectively. Equation (7c) represents a zero dispersive flux boundary, while (7d) and (7e) represent impervious boundaries. Because b is a stochastic variable, it follows that (3) is a stochastic partial differential equation. For every single realization of the aperture field, (3) subject to (7a)–(7e) is solved numerically by employing the fully implicit finite difference method, as outlined by Huyakorn and Pinder (1983) and Strikwerda (1989). A two-point backward difference approximation for the time derivative and a central difference approximation for the spatial derivatives are employed. The resulting approximation is second-order accurate.

Applying the resulting finite difference equation to each element in the fracture plane leads to a set of linear equations. By solving this set of equations in a similar fashion to the flow problem, the colloid concentration at each unit element is obtained.

2.3. CONTAMINANT TRANSPORT MODEL

The two-dimensional contaminant transport in a spatially variable aperture fracture in the presence of colloids, assuming that the contaminant may decay, sorb onto fracture surfaces as well as onto suspended and deposited colloids, and diffuse into the rock matrix; whereas, colloids may sorb onto fracture surfaces but may not penetrate the rock matrix (see Figure 1), is governed by the following partial differential equation:

$$(\text{Accumulation} = \text{Dispersion} - \text{Advection} - \text{Matrix diffusion} - \text{Decay})$$

$$\begin{aligned} & b\frac{\partial c}{\partial t} + 2(1-\epsilon)\frac{\partial c^*}{\partial t} + b\frac{\partial}{\partial t}(ns) + 2\frac{\partial}{\partial t}(n^* s^*) \\ & \quad = \nabla \cdot \Big[b\mathbf{D} \cdot \nabla(c + ns)\Big] - \nabla \cdot \Big[b\mathbf{U}(c + ns)\Big] - \\ & \qquad -2(1-\epsilon)q^* - \lambda\Big[bc + bns + 2(1-\epsilon)c^* + 2n^* s^*\Big], \end{aligned} \tag{8}$$

where $c(t, x, y)$ is the contaminant concentration in the fracture; $c^*(t, x, y)$ is the contaminant concentration adsorbed onto fracture surfaces, expressed as mass of contaminant per unit area of fracture surface; $s(t, x, y)$ is the contaminant concentration adsorbed on suspended colloids in the liquid phase, expressed as mass of contaminant per mass of colloids; $s^*(t, x, y)$ is the contaminant concentration adsorbed on deposited colloids, expressed as mass of contaminant per mass of deposited colloids; $\epsilon(t, x, y)$ is the fraction of the fracture surface physically covered by colloids; q^* is the diffusive mass flux of the contaminant in a direction perpendicular to the fracture plane; and λ is a first-order decay coefficient. Contaminant sorption onto fracture surfaces as well as diffusion into the rock matrix are dependent on the portion of the fracture surface area which is free of deposited colloids.

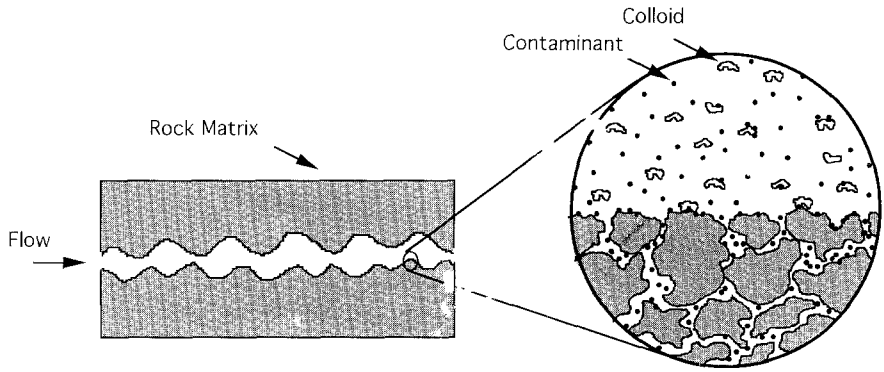

Fig. 1. Schematic illustration of contaminant transport in the presence of colloids in a spatially variable aperture fracture. Contaminants can sorb onto colloids as well as onto fracture surfaces and may diffuse into the rock matrix. Colloids deposit onto fracture surfaces but do not penetrate the rock matrix.

The stochastic transport equation (8) has been derived from a mass balance over a representative unit fracture. The first and second terms on the right-hand side of the preceding equation represent the dispersive and advective transport of the contaminant in solution and adsorbed on suspended colloids, respectively; the fourth term on the left-hand side, which is associated with $\partial n^* s^*/\partial t$, represents the deposition of colloidal particles with sorbed contaminant on their surfaces in conjunction with contaminant sorption onto deposited particles $(n^* s^* = (1-\epsilon)n^* s^* + \epsilon n^* s^*)$. It should be noted that for the derivation of (8) it is also assumed that contaminant sorption onto a colloidal particle does not alter the hydrodynamic and deposition mechanisms of the colloid. It is further assumed that the transport properties of the colloid-bound contaminant are altered to those of colloids. The hydrodynamic dispersion coefficient of colloidal particles is the sum of mechanical dispersion and Brownian diffusion, while for the case of dissolved contaminants it is the sum of mechanical dispersion and molecular diffusion. Generally, mechanical dispersion dominates Brownian diffusion and molecular diffusion. Therefore, the same hydrodynamic dispersion coefficient is used for both the contaminant and colloids.

Contaminant sorption onto fracture surfaces as well as onto suspended and deposited colloids is assumed to be governed by the following linear reversible equilibrium isotherms

$$c^*(t,x,y) = K_f c(t,x,y), \tag{9}$$

$$s(t,x,y) = K_n c(t,x,y), \tag{10}$$

$$s^*(t,x,y) = K_{n^*} c(t,x,y), \tag{11}$$

where K_f, K_n, and K_{n^*} are the partition coefficients for contaminant sorption onto fracture surfaces, suspended colloids, and deposited colloids, respectively. The diffusive mass flux normal to the fracture-matrix interface is expressed by

$$q^* = -\theta \mathcal{D}_m \left. \frac{\partial c_m(t,x,y,z)}{\partial z} \right|_{z=b/2}, \tag{12}$$

where θ is the porosity of the rock matrix; $\mathcal{D}_m$ is the effective diffusion coefficient in the rock matrix; c_m is the contaminant concentration in the rock matrix; and z is the coordinate perpendicular to the fracture plane. The reduction in contaminant sorption onto fracture surfaces, and contaminant diffusion into the rock matrix due to colloid deposition is accounted for by adjusting the value of $\epsilon(t,x,y)$ in every unit element. The value of ϵ ranges from a lower limit of zero for the case of no colloid deposition to an upper limit of one for complete monolayer colloid coverage ($0 \leq \epsilon \leq 1$). Assuming that colloidal particles are spherical and of equal size, the number of particles deposited per unit surface area of the fracture surface is calculated every time step by

$$N^*(t,x,y) = \frac{6n^*(t,x,y)}{\rho_p \pi d_p^3}, \tag{13}$$

where N^* is the number of particles per unit area; ρ_p is the density of particles; and d_p is the diameter of particles. The value of ϵ is evaluated by $\epsilon = (\pi d_p^2/4\alpha)(N^*/N^*_{\max})$, where $N^*_{\max}$ is the maximum number of colloidal particles per unit surface area, and it is determined using Equation (13) by replacing N^* and n^* with $N^*_{\max}$ and $n^*_{\max}$, respectively.

Substituting Equations (9)–(12) into (8) yields the final contaminant transport partial differential equation, the solution of which requires the time and space dependent colloid concentration in the fracture and contaminant concentration in the rock matrix. The colloid concentration in the fracture $n(t,x,y)$ is obtained by solving the system of governing equations presented in Section 2.2. Determination of $c_m(t,x,y,z)$ is obtained from the following one-dimensional partial differential equation governing contaminant diffusion in a direction perpendicular to the fracture plane, assuming that the interstitial liquid in the rock matrix is stationary and the contaminant undergoes decay and sorption onto the rock matrix

$$\frac{\partial c_m(t,x,y,z)}{\partial t} = \frac{\mathcal{D}_m}{R_m} \frac{\partial^2 c_m(t,x,y,z)}{\partial z^2} - \lambda c_m(t,x,y,z), \tag{14}$$

where R_m is the retardation factor in the rock matrix defined as

$$R_m = 1 + \frac{\rho_b K_m}{\theta}, \tag{15}$$

which implies that contaminant sorption onto rock-matrix solid surfaces is described by a linear reversible equilibrium isotherm; ρ_b is the bulk density of the rock matrix;

and $K_m = c_m^*/c_m$ is the contaminant partition coefficient in the rock matrix, defined as the mass of contaminant adsorbed per unit mass of solid rock matrix (c_m^*) divided by the contaminant concentration in the rock matrix (c_m).

The appropriate initial and boundary conditions for the contaminant transport equation (8) are obtained by replacing in Equation (7) $n(t, x, y)$ and n_o with $c(t, x, y)$ and c_o (constant contaminant concentration at the source), respectively. It is assumed that the contaminant and colloids are introduced simultaneously at the inlet boundary, and that c_o and n_o are in equilibrium at the boundary. This implies that at the source there is also a solid-phase contaminant concentration adsorbed onto suspended colloids (s_o). The final contaminant transport equation, resulting from substituting (9)–(12) into (8), is coupled together with (14) by imposing the following boundary conditions:

$$c_m(0, x, y, z) = 0, \quad c_m(t, x, y, b/2) = c(t, x, y), \tag{16a,b}$$

$$\frac{\partial c_m(t, x, y, \infty)}{\partial z} = 0. \tag{16c}$$

The numerical discretization for the contaminant transport model is obtained by employing the same finite difference approximation schemes used for the solution of the colloid transport model. The resulting set of linear equations is solved in a similar fashion to the colloid transport model, and yields the contaminant concentration at each unit element.

2.4. VALIDATION OF MODELS

The analytical solution to the one-dimensional version of the colloid transport model, introduced in Section 2.2, for a semi-infinite fracture idealized as two parallel plates with constant aperture subject to constant concentration inlet boundary condition has been presented by Abdel-Salam and Chrysikopoulos (1994)

$$n(t, x) = \frac{n_o}{2}\left\{\exp\left[\frac{Ux}{2D}(1-\xi)\right]\operatorname{erfc}\left[\frac{x - Ut\xi}{2(Dt)^{1/2}}\right] + \right.$$
$$\left. + \exp\left[\frac{Ux}{2D}(1+\xi)\right]\operatorname{erfc}\left[\frac{x + Ut\xi}{2(Dt)^{1/2}}\right]\right\}, \tag{17}$$

where

$$\xi = \left(1 + \frac{8\kappa D}{Ub^2}\right)^{1/2}. \tag{18}$$

Figure 2 shows a comparison between the numerical solution of the colloid transport model and the above analytical solution for two different fracture apertures at a distance $x = 5$ m downstream of the inlet boundary. It is clear from

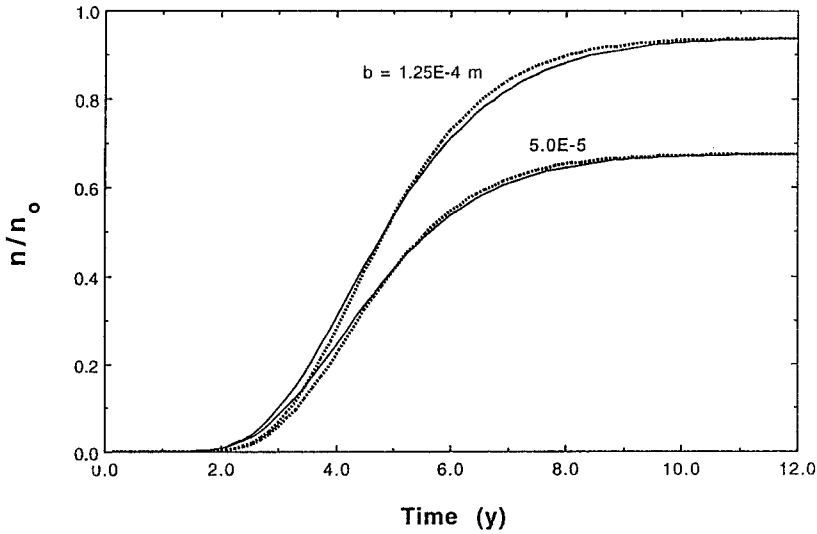

Fig. 2. Comparison between the analytical solution (broken lines) and numerical simulations (solid lines) of the colloid transport model for two different fracture apertures (Here $D = 0.25\,\mathrm{m^2/y}$, $U = 1.0\,\mathrm{m/y}$, $\kappa = 1.0 \times 10^{-10}\,\mathrm{m}$).

Figure 2 that very good agreement between the numerical and analytical solution is achieved. The breakthrough curves presented in Figure 2 do not reach the maximum value of relative concentration one, because some colloid mass is lost via irreversible deposition onto the fracture surfaces. Moreover, the liquid-phase colloid concentration decreases with decreasing fracture aperture, because a reduction in fracture aperture increases the accessibility of colloidal particles to the fracture surfaces, and leads to increased colloid deposition.

The numerical solution of the contaminant transport model, introduced in Section 2.3, is validated against the analytical solution of the following partial differential equation, which describes contaminant transport without the presence of colloids in a one-dimensional fracture idealized as two parallel plates with constant aperture

$$R\frac{\partial c(t,x)}{\partial t} = D\frac{\partial^2 c(t,x)}{\partial x^2} - U\frac{\partial c(t,x)}{\partial x} - \\ -R\lambda c(t,x) + \frac{2\theta \mathcal{D}_m}{b}\frac{\partial c_m(t,x,z)}{\partial z}\bigg|_{z=b/2}, \tag{19}$$

where R is the retardation factor in the fracture defined as

$$R = 1 + \frac{2K_f}{b}. \tag{20}$$

The analytical solution of Equation (19) for a semi-infinite fracture subject to constant concentration inlet boundary condition and using Equations (14)–(16) with $c_m(t, x, z)$ (independent of y), is given by (Tang *et al.*, 1981)

$$c(t,x) = \frac{c_o}{\pi^{1/2}} \int_{\eta}^{\infty} \exp\left[B - \zeta^2 - \frac{B^2}{4\zeta^2}\right] \times$$

$$\times \left\{ \exp\left[-\frac{\lambda R x^2}{4D\zeta^2} - \frac{\lambda^{1/2} A x^2}{4\zeta^2}\right] \operatorname{erfc}\left[\frac{Ax^2}{8\zeta^2 T^{1/2}} - (\lambda T)^{1/2}\right] + \right.$$

$$\left. + \exp\left[-\frac{\lambda R x^2}{4D\zeta^2} + \frac{\lambda^{1/2} A x^2}{4\zeta^2}\right] \operatorname{erfc}\left[\frac{Ax^2}{8\zeta^2 T^{1/2}} + (\lambda T)^{1/2}\right] \right\} \mathrm{d}\zeta, \qquad (21)$$

where

$$T = \left[t - \frac{Rx^2}{4D\zeta^2}\right], \quad A = \frac{2\theta}{bD}(R_m \mathcal{D}_m)^{1/2}, \qquad (22a,b)$$

$$B = \frac{Ux}{2D}, \quad \eta = \frac{x}{2}\left(\frac{R}{Dt}\right)^{1/2}, \qquad (22c,d)$$

and ζ is a dummy integration variable. A comparison between the numerical and the analytical solution for two different partition coefficients for contaminant sorption onto fracture surfaces K_f is presented in Figure 3. The two solutions are in very good agreement. Figure 3 also illustrates that the contaminant concentration in solution increases with decreasing K_f, because the contaminant mass sorbing onto the fracture surfaces reduces (see (9)).

3. Simulations and Discussion

3.1. FLOW

The hypothetical fracture used in this work has dimensions $\ell_x = 8$ m and $\ell_y = 4$ m, and it is partitioned into 80 × 40 uniform unit elements of equal size. The fracture aperture is assumed lognormally distributed with mean 1.65 μm and standard deviation 0.45. These values are approximately equal to those used by Moreno *et al.* (1988). The assumption of lognormally distributed aperture fluctuations is in agreement with measured apparent apertures from selective cores and well logs (Bianchi and Snow, 1968), apertures derived from permeability tests in granite (Bourke *et al.*, 1985), and aperture measurements of laboratory core samples (Gale, 1982; Hakami and Barton, 1990). Here, an isotropic exponential autocovariance function is employed with a correlation scale of 0.3 m. The aperture size ranges from 3 μm to 200 μm.

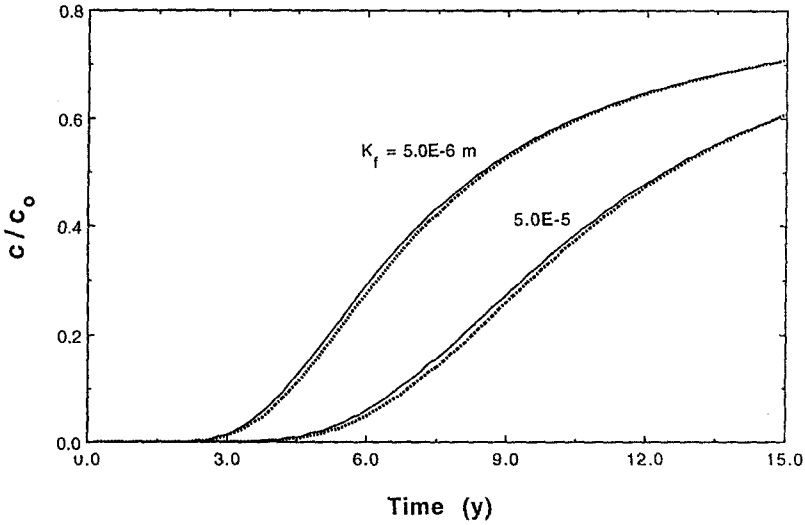

Fig. 3. Comparison between the analytical solution (broken lines) and numerical simulations (solid lines) of the contaminant transport model without the presence of colloids for two different partition coefficients for contaminant sorption onto fracture surfaces (Here $b = 1.25 \times 10^{-4}$ m, $D = 0.25\,\mathrm{m^2/y}$, $U = 1.0\,\mathrm{m/y}$, $\mathcal{D}_m = 1.0 \times 10^{-6}\,\mathrm{m^2/y}$, $\lambda = 1.0 \times 10^{-6}\,1/\mathrm{y}$).

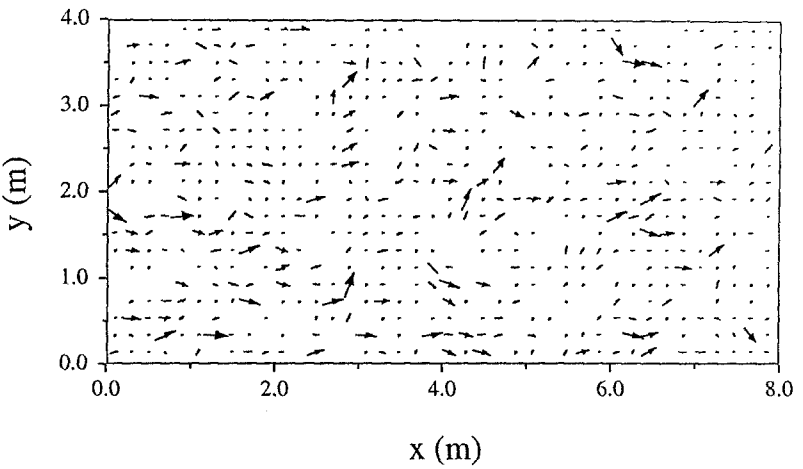

Fig. 4. Velocity vector field in the fracture plane for a single realization of the aperture field. Arrow lengths are proportional to velocity magnitudes.

Figure 4 shows a plot of the velocity vector field in the fracture plane for a single realization of the aperture field. The constant head gradient imposed on the flow model is 3.0×10^{-5}. This value represents a 1.72 m/y velocity in a fracture with constant aperture of 45 μm (this is the mean of the assumed lognormal distribution). The length of each arrow is proportional to the magnitude of the resultant velocity, with values ranging between 0.4–4.0 m/y. Velocities below 0.4 m/y and above

TABLE I. Typical parameter values for the transport models

Parameter	Value	References
$\mathcal{D}_m$	1.0×10^{-6} m^2/y	Skagius and Neretnieks (1986)
K_f	1.0×10^{-4} m	KBS-3 (1983)
K_n	5.0×10^{-3} m^3/g	
K_{n^*}	1.0×10^{-5} m^3/g	
α_L	0.2 m	
α_T	0.02 m	
θ	0.003	Abelin (1986)
κ	1.0×10^{-10} m	Bowen and Epstein (1979), Toran and Palumbo (1992)
λ	1.0×10^{-6} 1/y	Abelin (1986)
ρ_b	2.0×10^{6} g/m^3	Skagius and Neretnieks (1986)

4.0 m/y are not shown. Since the velocity is proportional to the aperture squared and the head gradient, high velocities are found within elements with large aperture size and/or large head gradient.

3.2. COLLOID TRANSPORT WITH AND WITHOUT SIZE EXCLUSION

For fractures with spatially variable aperture, it is expected that colloids will bypass small size elements by following the least resistive pathways. This phenomenon is known as size exclusion. In order to understand and evaluate the effect of size exclusion on colloid transport and ultimately on contaminant transport, we investigated colloid transport for both cases of with and without size exclusion. Simulations are conducted using the numerical solution of the colloid transport equation (3), which does not account for particle entrapment between the fracture surfaces. With the exception of α_L and α_T the parameter values used in the colloid transport model simulations have been obtained from Bowen and Epstein (1979) and Toran and Palumbo (1992), and they are listed in Table I. The grid-Péclet-numbers, $\mathrm{Pe}_x = U_x\Delta x/D_{xx}$, and $\mathrm{Pe}_y = U_y\Delta y/D_{yy}$ in the x- and y-directions, respectively (Kinzelbach, 1986), ranged from 0.01 to 1.67. This range is in agreement with the recommendation by Kinzelbach (1986) who suggested that grid-Peclet-numbers should be < 2, in order to avoid numerical problems.

Figure 5 shows a comparison between colloid concentration in the fracture plane with and without size exclusion for a single realization after six years of simulation time. The scale in Figure 5 ranges from black representing high concentration ($n/n_o = 1$) to white representing low concentration ($n/n_o = 0$). The two-dimensional snapshot in Figure 5a portrays the colloid concentration where colloids are allowed to travel throughout the whole fracture plane. Because of the

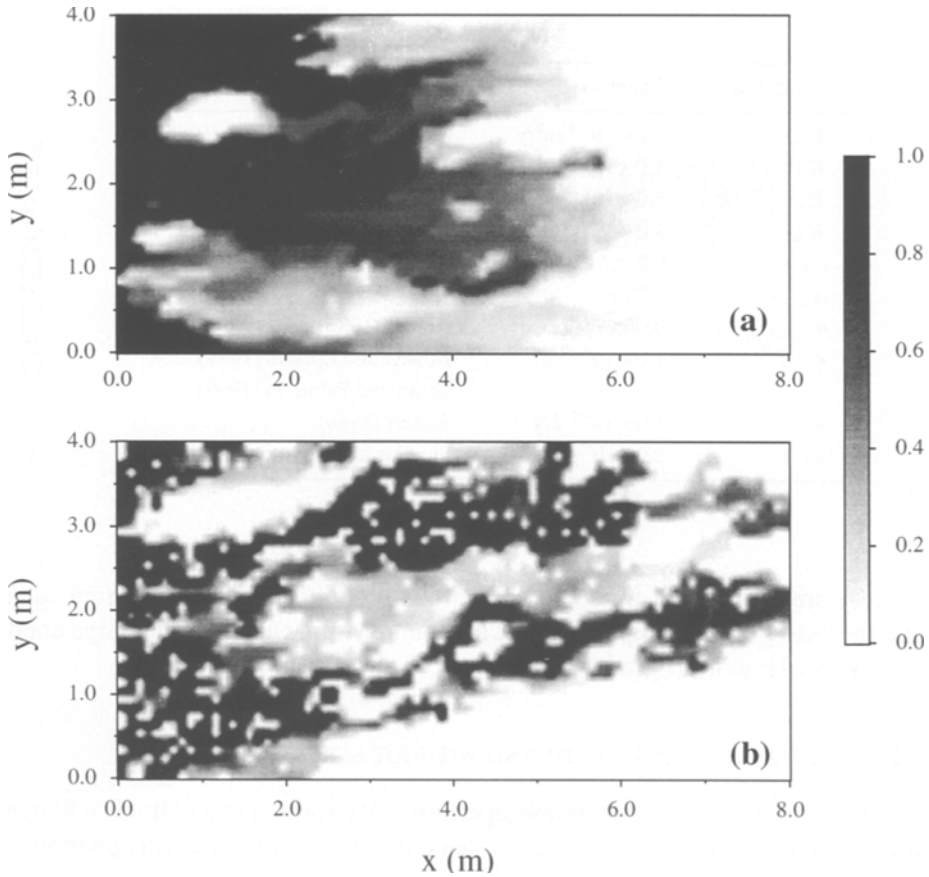

Fig. 5. Spatial distribution of normalized suspended colloid concentration in the fracture plane, for transport: (a) without size exclusion and (b) with size exclusion. The colloid source is uniformly distributed across the entire width of the inlet boundary (Here $t = 6$ y).

variable aperture nature of the fracture, formation of some fingering occurs. In Figure 5b, colloids are restricted from entering elements with apertures smaller than 15 μm, assuming that colloidal particles are spherical and of equal diameter (1 μm) so that the possibility of particle straining is eliminated (Sakthivadivel, 1969; and Herzig *et al.*, 1970). No-flow elements are simulated by setting both the advective and dispersive fluxes into these elements to zero. It is clear from Figure 5b that size exclusion leads to faster breakthrough and more pronounced fingering. The small white spots in Figure 5b represent the no-flow elements. Similar results have been observed for the special case where the colloid source does not cover the whole fracture width, but 0.4 m at the center of the inlet boundary (see Figure 6).

Because the governing colloid transport equation is stochastic, the effect of size exclusion on colloid transport is best illustrated by comparing both cases of colloid transport with and without exclusion for the ensemble average (i.e.,

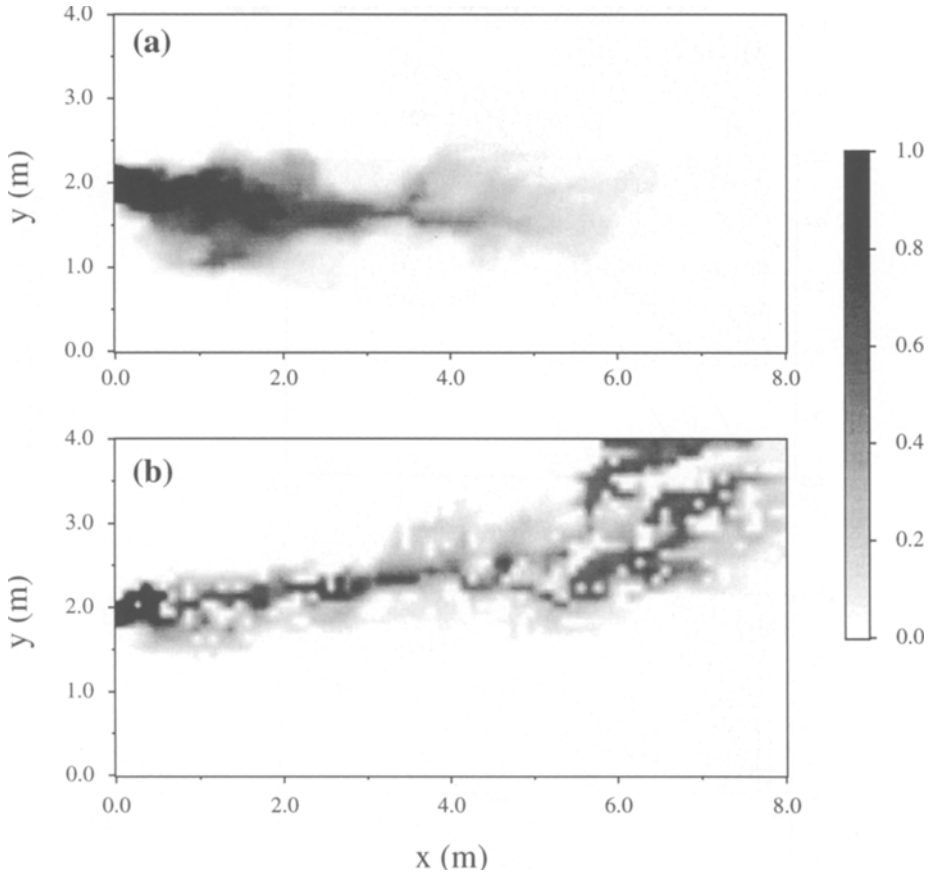

Fig. 6. Spatial distribution of normalized suspended colloid concentration in the fracture plane, for transport: (a) without size exclusion and (b) with size exclusion. The colloid source is 0.4 m wide at the center of the inlet boundary (Here $t = 6$ y).

expected value) of several realizations. The ensemble breakthrough curves shown in Figure 7 are based on 60 realizations for colloid concentration averaged across the fracture width at 3 and 4 m downstream from the inlet boundary. The number of realizations is chosen such that additional realizations do not change the calculated ensemble average. Figures 7a and 7b indicate that size exclusion leads to an earlier breakthrough of colloids and that the difference in breakthrough time increases with distance downstream from the source. The long tailing of the breakthrough curves for colloids with size-exclusion and the intersection between the curves corresponding to the cases of with and without size exclusion presented in Figure 7, indicate that size exclusion enhances the dispersion of colloids.

The impact of standard deviation σ of the lognormally distributed fluctuations of the fracture aperture on the ensemble average breakthrough curve, based on 60 realizations, for colloid transport with size exclusion is shown in Figure 8. It

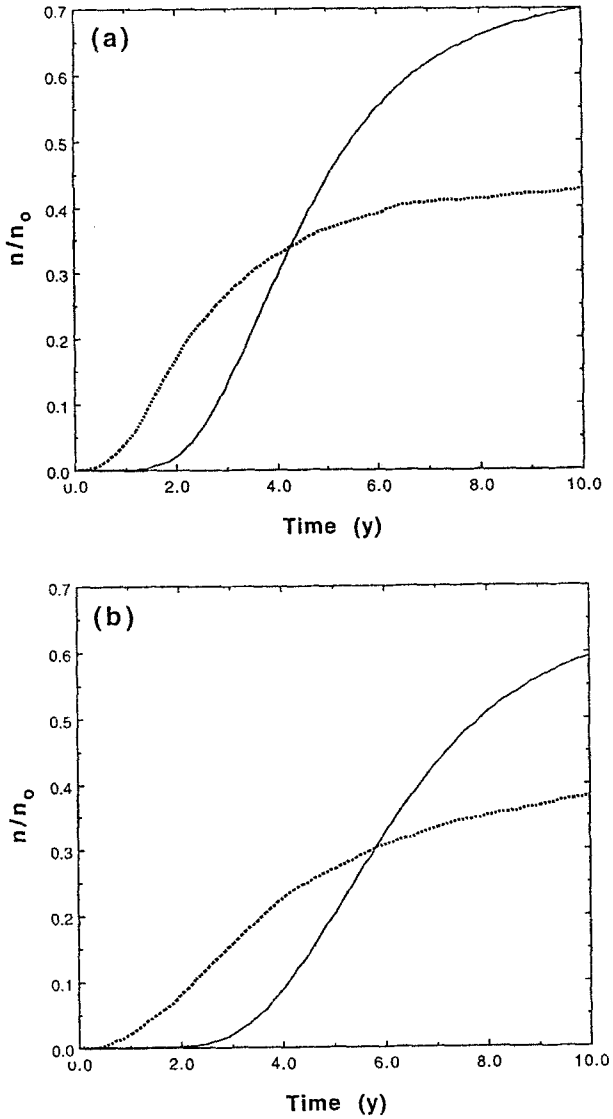

Fig. 7. Temporal distribution of normalized suspended colloid concentration for an ensemble average of 60 realizations at a distance of: (a) 3.0 m and (b) 4.0 m downstream of the source. Solid lines represent transport without size exclusion and broken lines represent transport with size exclusion.

is clear that increasing the standard deviation leads to an earlier breakthrough of colloids. This is because, increasing σ leads to a greater variability in the aperture distribution within the fracture plane, which in turn contributes to the preferential transport of colloids, and consequently increases the dispersion of colloids. An

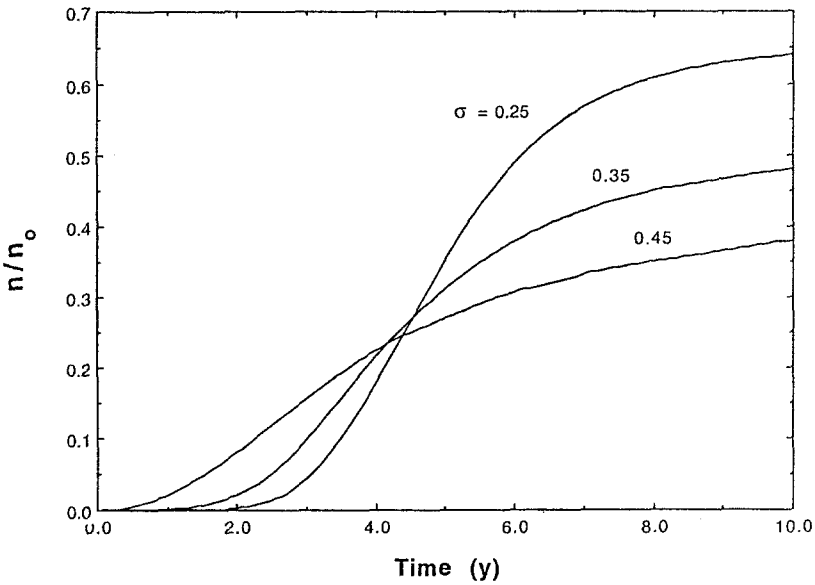

Fig. 8. Temporal distribution of normalized suspended colloid concentration for an ensemble average of 60 realizations at a distance of 4.0 m downstream of the source for three different standard deviations of the aperture fluctuations and with colloids subjected to size exclusion.

increase in σ also yields similar results for the case of colloid transport without size exclusion.

3.3. CONTAMINANT TRANSPORT IN THE PRESENCE AND ABSENCE OF COLLOIDS

Colloid-facilitated transport is dependent mainly on the liquid-phase colloid concentration, colloid deposition rate, and the interaction between the contaminant and colloids. Simulations based on the previously presented contaminant transport model in the absence and presence of colloids are conducted with parameter values, other than the colloid transport model parameters, obtained from KBS-3 (1983), Abelin (1986), and Skagius and Neretnieks (1986). These parameter values are listed in Table I. The contaminant source concentration c_o is assumed to be equal to the colloid source concentration n_o. The dissolved contaminant is not expected to be subject to size exclusion, and consequently it is expected to sample every unit element of the fracture plane, because its molecular size is 7–10 orders of magnitude smaller than the size of colloids. Nevertheless, contaminant sorbed onto colloidal particles is subjected to colloid transport behavior and it is affected by size exclusion. Figure 9 shows a two-dimensional snapshot corresponding to a single aperture field realization for contaminant transport in the absence (Figure 9a) and presence of colloids (Figure 9b), where colloids are subject to size exclusion. It is clear from this figure that, for the set of parameters considered, the presence of colloids enhanced contaminant transport.

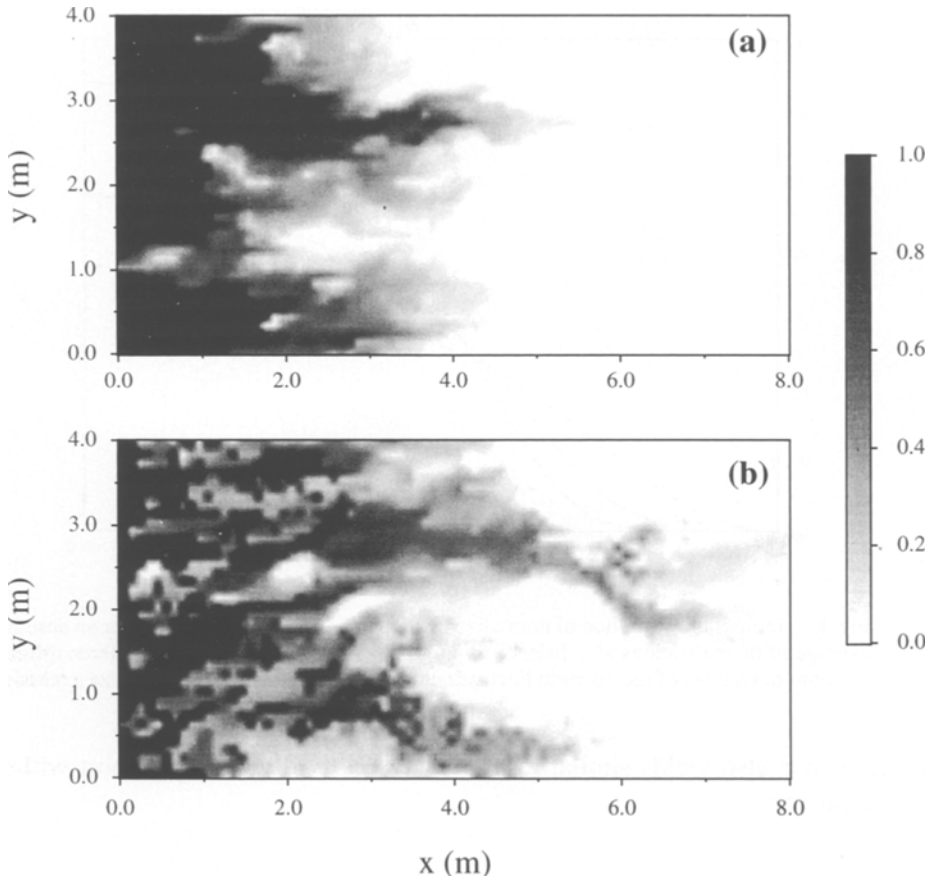

Fig. 9. Spatial distribution of normalized liquid-phase contaminant concentration in the fracture plane: (a) in the absence of colloids and (b) in the presence of colloids. The contaminant and colloid sources are uniformly distributed across the entire width of the inlet boundary (Here $t = 6$ y).

Figure 10 presents ensemble breakthrough curves for contaminant transport in the absence and presence of colloids, with colloids subjected to size exclusion. The curves are based on 60 realizations for contaminant concentration averaged over the fracture width at a distance 3 and 4 m downstream from the inlet boundary. It is clear from Figure 10 that the presence of colloids leads to an earlier contaminant breakthrough and increased contaminant dispersion. This is demonstrated in Figure 10 by the long tailing of the breakthrough curves corresponding to the case where colloids are present.

The effect of the partition coefficient for contaminant sorption onto suspended colloids K_n on contaminant transport in the presence of colloids subjected to size exclusion is shown in Figure 11. The breakthrough curves presented in Figure 11 are based on an ensemble average of 60 realizations. It is clear that increasing K_n

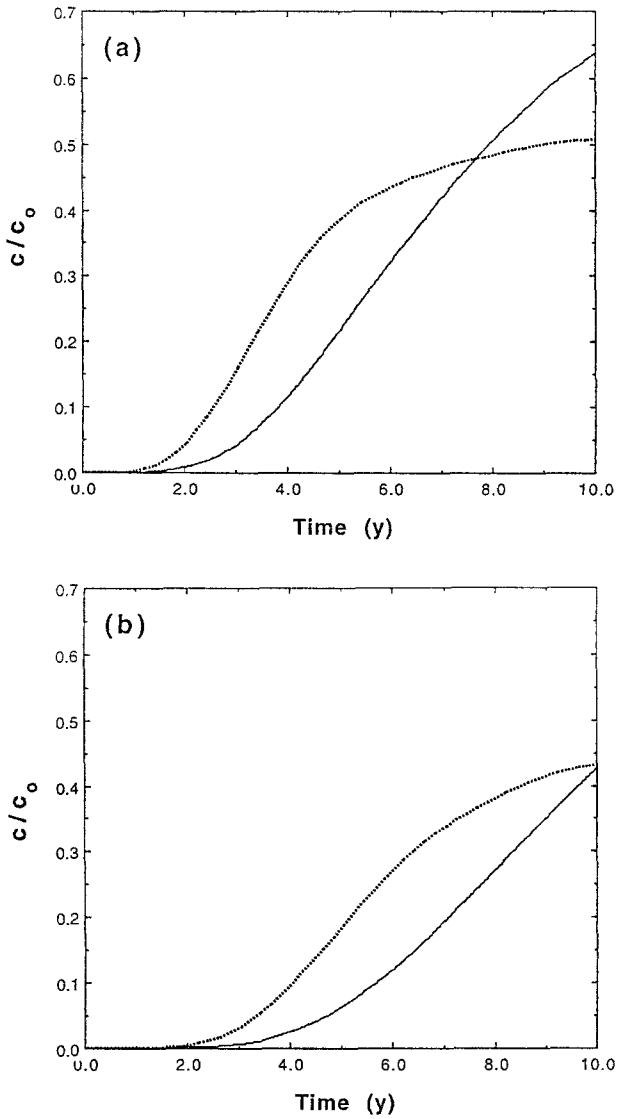

Fig. 10. Temporal distribution of normalized liquid-phase contaminant concentration for an ensemble average of 60 realizations at a distance of (a) 3.0 m and (b) 4.0 m downstream of the source. Solid lines represent transport in the absence of colloids and broken lines represent transport in the presence of colloids.

leads to an earlier breakthrough of the contaminant. This could be attributed to the increase of contaminant sorption onto suspended colloids, which in turn decreases contaminant retardation by sorption onto the fracture surfaces and by diffusion into the rock matrix.

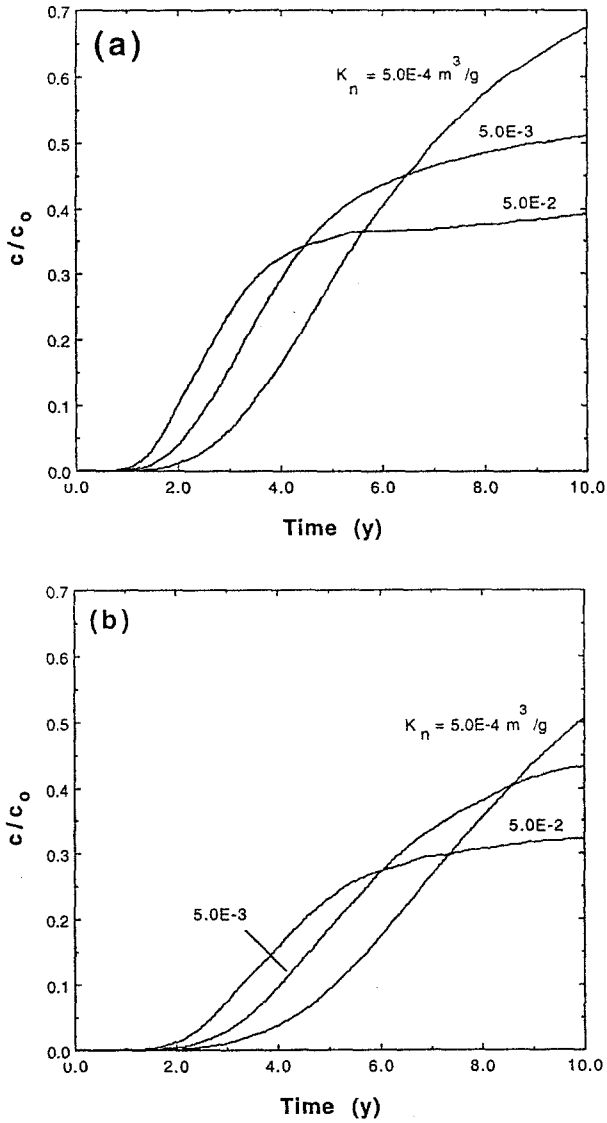

Fig. 11. Effect of partition coefficient for contaminant sorption onto suspended colloids on temporal distribution of normalized liquid-phase contaminant concentration for an ensemble average of 60 realizations at a distance of (a) 3.0 m and (b) 4.0 m downstream of the source.

4. Summary and Conclusions

This work focuses on the analysis of colloid and colloid-facilitated contaminant transport in a two-dimensional fracture-rock matrix system with a spatially variable aperture and homogeneous, isotropic rock matrix. First, several random realizations of the velocity field in the fracture plane were generated assuming that the fracture

aperture is a stochastic variable. Then, a colloid transport model accounting for irreversible colloid deposition onto fracture surfaces was developed. Finally, a comprehensive model of contaminant transport in the presence of colloids was presented, accounting for reversible contaminant sorption onto fracture surfaces and onto suspended as well as deposited colloids, and allowing for contaminant diffusion into the rock matrix and first order decay.

Several model simulations indicate that a fracture with spatially variable aperture causes the contaminant and colloids to follow preferential paths within the fracture plane. Faster transport and more pronounced fingering of colloids are observed when colloids are excluded from elements in the fracture plane with small aperture size. Similar results are obtained for the special case where the colloid source is only 0.4 m wide at the center of the inlet boundary. Size exclusion also increases the dispersion of colloids. Moreover, it is shown that, for the parameter set considered, colloids enhance the transport of contaminants and yield long tailed contaminant breakthrough curves.

Although, the models presented provide very good means of predicting and analyzing the effect of spatially variable aperture on colloid and colloid-facilitated contaminant transport, some of the limitations inherent to the models are their inability to account for (a) kinetic sorption between the contaminant and colloids; (b) particle entrapment between the fracture surfaces; and (c) reduction in permeability because of colloid deposition onto fracture surfaces. Nonetheless, this work can provide a starting point for generalization to the solution of more complicated physical systems.

Acknowledgements

The authors acknowledge Gary Litton for many stimulating discussions. A. A.-S. is grateful for the support provided by the UCI Regents Dissertation Fellowship. This work has been supported in part by the UCI Academic Senate Committee on Research under faculty research award IRF-95.

References

Abdel-Salam, A. and Chrysikopoulos, C. V.: 1994, Analytical solutions for one-dimensional colloid transport in saturated fractures, *Advances in Water Resour.* **17**(5), 283–296.

Abelin, H.: 1986, Migration in a single fracture: An in situ experiment in a natural fracture, Ph.D. dissertation, Dep. of Chem. Eng., R. Inst. of Tech., Stockholm, 170 pp.

Bear, J. and Verruijt, A.: 1987, *Modeling Groundwater Flow and Pollution*, D. Reidel, Dordrecht.

Bianchi, L. and Snow, D.: 1968, Permeability crystalline rock interpretated from measured orientations and apertures of fractures, *Ann. Arid Zone* **8**(2), 231–245.

Bourke, P. J., Dunance, E. M., Heath, M. J. and Hodgkinson, D. D.: 1985, Fracture hydrology relevant to radionuclide transport, AERE Rep. 11414, Atomic Energy Res. Estab., Harwell, United Kingdom.

Bourke, P. J.: 1987, Channeling of flow through fractures in rock, *Proceedings, GEOVAL87 Symposium*, Swed. Nucl. Power Inst., Stockholm, pp. 167–177.

Bowen, B. D. and Epstein, N.: 1979, Fine particle deposition in smooth parallel-plate channels, *J. Colloid and Interface Sci.* **72**(1), 81–97.

Bradbury, M. H. and Green, A.: 1986, Investigations into the factors influencing long range matrix diffusion rates and pore space accessibility at depth in granite, *J. Hydrol.* **89**, 123–139.

Buddemeier, R. W. and Hunt, J. R.: 1988, Transport of colloidal contaminants in groundwater radionuclide migration at the Nevada test site, *Appl. Geochem.* **3**, 535–548.

Champ, D. R. and Schroeter, J.: 1988, Bacterial transport in fractured rock: A field-scale tracer test at the Chalk River Nuclear Laboratories, *Water Sci. Technol.* **20**(11/12), 81–87.

Enfield, C. G. and Bengtsson, G.: 1988, Macromolecular transport of hydrophobic contaminants in aqueous environments, *Ground Water* **26**(4) 64–70.

Enfield, C. G., Bengtsson, G. and Lindqvist, R.: 1989, Influence of Macromolecules on chemical transport, *Environ. Sci. Technol.* **23**(10) 1278–1286.

Gale, J. E.: 1982, The effects of fracture type (induced versus natural) on the stress-fracture closure-fracture permeability relationships, in *Proceedings at 23rd Symposium on Rock Mechanics*, Univ. Calif., Berkeley, pp. 290–298.

Gale J. E., Rouleau, A. and Atkinson, L. C.: 1985, Hydraulic properties of fractures, *Proceedings, Int. Assoc. of Hydrogeologists, Memoirs*, Tucson Congress **17** pp. 1–11.

Grisak, G. E. and Pickens, J. F.: 1981, An analytical solution for solute transport through fractured media with matrix diffusion, *J. Hydrol.* **52**, 47–57.

Hakami, E. and Barton, N.: 1990, Aperture measurements and flow experiments using transparent replicas of rock joints, in N. Barton and O. Stephansson (eds), *Rock Joints*, A. A. Balkema, Rotterdam, pp. 383–390.

Haldeman, W. R., Chuang, Y., Rasmussen, T. C. and Evans, D. D.: 1991, Laboratory analysis of fluid flow and solute transport through a fracture embedded in porous tuff, *Water Resour. Res.* **27**(1), 53–65.

Harvey, R. W., George, L. H., Smith, R. L. and LeBlanc, D. R.: 1989, Transport of fluorescent microshpere and indigenous bacteria through a sandy aquifer: Results of natural- and forced-gradient tracer experiment, *Environ. Sci. Technol.* **23**, 51–56.

Harvey R. W. and Garabedian, S. P.: 1991, Use of colloid filtration theory in modeling movement of bacteria through a contaminated sandy aquifer, *Environ. Sci. Technol.* **25**, 178–185.

Herzig, J. P., Leclerc, D. M. and Le Goff, P.: 1970, Flow of suspension through porous media: Application to deep filtration, *Ind. Eng. Chem.* **62**(5), 9–35.

Higgo, J. J. W., Williams, G. M., Harrison, I., Warwick, P., Gardiner, M. P. and Longworth, G.: 1993, Colloid transport in a glacial sand aquifer. Laboratory and field studies, *Colloids and Surfaces A* **73**, 179–200.

Huyakorn, P. S. and Pinder, G. F.: 1983, *Computational Methods in Subsurface Flow*, Academic Press, New York.

Johns, R. A. and Roberts, P. V.: 1991, A solute transport model for channelized flow in a fracture, *Water Resour. Res.* **27**(8), 1797–1808.

KBS–3, 1983, Final storage of spent nuclear fuel, 4, technical report, Swedish Nuclear Fuel Supply, 124 pp.

Kinzelbach, W.: 1986, *Developments in Water Science, Groundwater Modelling*, Elsevier, Amsterdam.

Krishnamoorthy, T. M., Nair, R. N. and Sarma, T. P.: 1992, Migration of radionuclides from a granite repository, *Water Resour. Res.* **28**(7), 1927–1934.

Lapidus, L. and Pinder, G.: 1982, *Numerical Solution of Partial Differential Equations in Science and Engineering*, Wiley, New York.

McCarthy, J. F. and Zachara, J. M.: 1989, Subsurface transport of contaminants, *Environ. Sci. Technol.*, **23**(5), 496–502.

Moreno, L., Tsang, Y. W., Tsang, C. F., Hale, F. V. and Neretnieks, I.: 1988, Flow and tracer transport in a single fracture: A stochastic model and its relation to some field observations, *Water Resour. Res.* **24**, 2033–2048.

Moulin, V. and Ouzounian, G.: 1992, Role of colloids and humic substances in the transport of radio-elements through the geosphere, *Appl. Geochem. Suppl. Issue* (1), 179–186.

Neretnieks, I., Eriksen, T. and Tahtinen, P.: 1982, Tracer movement in a single fissure in granitic rock: Some experimental results and their interpretation, *Water Resour. Res.* **18**, 849–858.

Neretnieks, I.: 1983, A note on fracture flow dispersion mechanisms in the ground, *Water Resour. Res.* **23**, 561–570.

Neretnieks, I.: 1985, Transport in fractured rocks, *Proceedings, Int. Assoc. of Hydrogeologists, Memoirs, Tucson Congress* **17**, pp. 301–318.

Neuzil, C. E. and Tracy, J. V.: 1981, Flow through fractures, *Water Resour. Res.* **17**, 191–199.

Novakowski, K. S., Evans, G. V., Lever, D. A. and Raven, K.: 1985, A field example of measuring hydrodynamic dispersion in a single fracture, *Water Resour. Res.* **21**, 1165–1174.

Press, W. H., Teukolsky, S. A., Vetterling, W. T. and Flannery, B. P.: 1992, *Numerical Recipes in Fortran: The Art of Scientific Computing*, Cambridge University Press.

Puls, R. W., Paul, C. J. and Clark, D. A.: 1993, Surface chemical effects on colloid stability and transport through natural porous media, *Colloids and Surfaces A* **73**, 287–300.

Pyrak, L. R., Myer, L. R. and Cook, N. G. W.: 1985, Determination of fracture void geometry and contact area at different effective stress, *Eos Trans. AGU* Abstract, **66**(46), 903.

Raven, K. G., Novakowski, K. S. and Lapeciv, P.A.: 1988, Interpretation of field tracer tests of a single fracture using a transient solute storage model, *Water Resour. Res.* **24**, 2019–2032.

Sakthivadivel, R.: 1969, Clogging of a granular porous medium by sediment, Hydraul. Eng. Lab., Univ. of Calif., Berkeley, Rep. HEL 15-17, 106 pp.

Schrauf, T. W. and Evans, D. D.: 1986, Laboratory studies of gas flow through a single natural fracture, *Water Resour. Res.* **22**, 1038–1050.

Shapiro, A. M. and Nicholas, J. R.: 1989, Estimating the statistical properties of fracture aperture using field scale hydraulic and tracer tests: Theory and application, *Water Resour. Res.* **25**, 817–828.

Skagius, K. and Neretnieks, I.: 1986, Porosities and diffusivities of some nonsorbing species in crystalline rocks, *Water Resour. Res.* **22**(3), 389–398.

Sposito, G.: 1984, *The Surface Chemistry of Soils*, Oxford University Press, New York.

Song, L. and Elimelech, M.: 1993, Dynamics of colloid deposition in porous media: Modeling the role of retained particles, *Colloids and Surfaces A* **73**, 49–63.

Streltsova, T. D.: 1988, *Well Testing in Heterogeneous Formations*, Wiley, New York.

Strikwerda, J. C.: 1989, *Finite Difference Schemes and Partial Differential Equations*, Wadsworth & Brooks/Cole.

Tang, D. H., Frind, E. O. and Sudicky, E. A.: 1981, Contaminant transport in fractured porous media: Analytical solution for a single fracture, *Water Resour. Res.* **17**(3), 555–564.

Toran, L. and Palumbo, A. V.: 1992, Colloid transport through fractured and unfractured laboratory sand columns, *J. Contam. Hydrol.* **9**, 289–303.

Tsang, Y. W. and Tsang, C. F.: 1987, Channel model of flow through fractured media, *Water Resour. Res.* **23**, 467–479.

Williams, S. A. and El-Kadi, A. I.: 1986, COVAR: A computer program for generating two-dimensional fields of autocorrelated parameters by matrix decomposition, *Int. Groundwater Model. Cent.*, Holcomb Res. Inst., Colorado School of Mines, Golden, CO.

Witherspoon, P. A., Wang, J. S. Y., Iwai, K. and Gale, J. E.: 1980, Validity of cubic law for fluid flow in a deformable rock fracture, *Water Resour. Res.* **16**(6), 1016–1024.